On the Modeling of Quasi-Steady and Unsteady Dynamic Friction in Sliding Lubricated Line Contact

H. Sojoudi

M. M. Khonsari[1]
Dow Chemical Endowed Chair in Rotating Machinery
Fellow ASME
e-mail: khonsari@me.lsu.edu

Department of Mechanical Engineering,
Louisiana State University,
Patrick Taylor Hall,
Baton Rouge, LA 70803

A simple but realistic dynamic friction model for the lubricated sliding contact is developed based on decoupling the steady and unsteady terms in Reynolds equation. The model realistically captures the physics of friction behavior both when speed is increased unidirectionally or when operating under oscillating condition. The model can simulate the transition from boundary to mixed to full film regimes as the speed is increased. Two different classes of simulations are performed to show the utility of the model: the so-called quasisteady, where the sliding velocity is varied very slowly, and the oscillating sliding velocity, where the friction coefficient exhibits a hysteresis type behavior. Both categories of simulation are verified by comparing the results with published experimental data. [DOI: 10.1115/1.4000272]

Keywords: unsteady friction, oscillatory friction, hysteresis effect

1 Introduction

When a system operates under dynamic conditions such as variable speed, oscillating velocity, and oscillating load, the behavior of the friction coefficient is not only a function of velocity, but also a function of velocity history. Variable friction under unsteady conditions is often referred to as dynamic friction. The behavior of dynamic friction has been observed by several investigators. Hess and Soom [1] conducted a series of experiments to measure friction in a line contact configuration subjected to oscillatory velocity. Their experimental results show a characteristic time lag between the changing velocity and the corresponding steady-state friction. This lag between oscillating friction and velocity in lubricated surfaces was observed earlier by Rabinowicz [2] in dealing with dry contacts. Empirical results for lubricated dynamic friction reported by Harnoy et al. [3] reveal similar results. Lu and Khonsari [4] performed an experimental study for the grease-lubricated journal bearing undergoing oscillatory motion. They reported how the changes in the applied force could affect the friction coefficient in different oscillating frequencies. In another work [5], they repeated the experiments in an oil-lubricated journal bearing and investigated how the oil type, oil temperature, applied load, and oscillating frequency influences the friction coefficient.

In the classical hydrodynamic lubrication theory, the lubrication film thickness is increasing with velocity. Consequently, upon increasing the velocity, the lubrication regimes changes from boundary lubricated to the mixed lubrication, in which both the surface roughness and fluid film contribute to the load-carrying capacity. Roughness effects in elastohydrodynamic lubrication (EHL) have captured the attention of many researchers. For this purpose, the problem of surface waviness is commonly considered as an important step toward the understanding the lubrication of rough surfaces. Greenwood and Johnson [6] conducted an elementary analysis of the process of transverse roughness, which allows the estimation of pressure ripples that occur due to waviness. Later, Greenwood and Morales-Espejel [7] investigated the behavior of transverse roughness in EHL contacts. In a follow-up study, they considered a complementary function for the amplitude of waviness [8]. A full numerical solution of an EHL problem in rolling/sliding lubricated contact is performed by Lubrecht et al. [9], who considered the waviness effect of the surface pattern on film thickness and surface deformation. They urged the need to study the waviness effect on the elastic deformation due to highly increasing demand for a decrease in the film thickness in practice. Amplitude of the wavelength is decreased while the mating surfaces are passing through an EHL conjunction and the effect of operating conditions is investigated on this reduction. The behavior is investigated both when the surfaces are under pure rolling and there is a combination of sliding and rolling. A detail study of EHL line and point contact is performed by Venner and Lubrecht [10], investigating the influence of operating conditions such as the oil inlet and wavelength on the surface pattern. During the operation of the system, a change in the parameters of the surface roughness occurs, which influences the behavior of EHL problem. When a waviness pattern passes through an EHL conjunction, the wavelength increases while the amplitude decreases and new wave patterns is produced. The starvation effect on the attenuation of surface roughness is investigated for a surface with transverse roughness pattern [10,7]. Hooke and Venner [11] compared the effect of roughness in EHL line and point contact. Both types of conjunction show the identical behavior in terms of surface attenuation.

The steady-state friction of lubricated sliding surfaces plotted as a function of velocity reduces to what tribology literature refers to as the Stribeck curve [12]. The full lubrication regime occurs when the sliding velocity is above a transition value required to generate a lubrication film thicker than the size of the surface asperities. The nature of Stribeck curve has been investigated by many researchers. In the recent work, Lu et al. [13] used the so-called Johnson's load-sharing concept [14] in order to predict the Stribeck curve. They showed that the simulation results are in good agreement with the experiments, especially in the mixed regime. In the present study, we extend the theory to predict the friction coefficient in boundary, mixed and full film regimes during an increasing velocity.

The term EHL refers to lubrication studies, where the surface deformations due to high film pressure are taken into account. Also important in EHL is the consideration of the appropriate rheological characteristic and its dependence on pressure. Treatment of EHL requires solving the Reynolds equation, appropriate rheology equation, and elasticity equation. A comprehensive study is reported by Pan and Hamrock [15]. More recently, Moes [16]

[1]Corresponding author.

Contributed by the Tribology Division of ASME for publication in the JOURNAL OF TRIBOLOGY. Manuscript received March 12, 2009; final manuscript received August 27, 2009; published online November 11, 2009. Assoc. Editor: Michael D. Bryant.

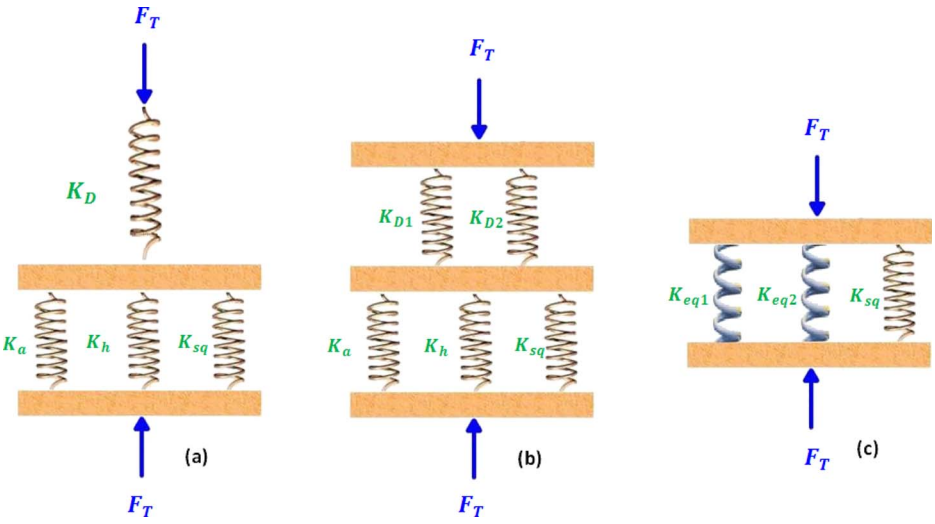

Fig. 1 (*a*) **Schematic representation of an unsteady EHL contact;** (*b*) **equivalent system of** (*a*) ($K_D = K_{D1} + K_{D2}$); (*c*) **equivalent system of** (*a*) **and** (*b*) ($1/K_{eq1} = 1/K_{D1} + 1/K_a$ **and** $1/K_{eq2} = 1/K_{D2} + 1/K_h$)

introduced an optimum similarity analysis with applications to EHL. In the current study, we make use of the relationship provided by Moes, recognizing that the approach is restricted to smooth surfaces.

Asperity interaction is unavoidable for the lubricated line contact, especially under highly loaded operating conditions. Greenwood and Williamson [17] proposed a statistical representation of surface roughness to calculate the separation, nominal area, and pressure between two interacting surfaces. Gelinck and Schipper [18] used the equation for the load between asperities, considering the deformation equation in the line contact in order to relate the mean asperity pressure to the maximum Hertzian pressure. Later, they used it to predict the behavior of friction in the Stribeck curve for line contact [19]. This approach was used by Lu et al. [13], who experimentally verified its validity, and extended in a follow-up study by Akbarzadeh and Khonsari [20], who applied it to gear lubrication. Nevertheless, the published results using this method are limited to mixed lubrication with constant unidirectional velocity in line contact without hysteresis.

The hysteresis phenomenon is not limited to line contact configuration. Harnoy and Friedland [21] proposed a model to simulate the dynamic friction coefficient in a short journal bearing operating in a conformal contact. Rachoor and Harnoy extended the idea to other geometries in Ref. [22]. The approach used in developing the model was based on treating the elastic deformation behavior of contacting asperities as a linear spring. They quantified the spring stiffness through fitting the simulation results to those of steady-state experiments. This approach requires conducting a series of steady-state experiments in order to predict dynamic friction behavior. Thus, if experimental results are available, this approach would be useful for designing control systems and is particularly attractive because of its simplicity. The research is motivated by the need of a model-based control system, where the dynamic friction is required in the control algorithm. The desire for simplicity of the model for application in control systems stems from the "real-time" friction compensation requirement in devices that demand precision motion. Canudas de Witt et al. [23] and Olsson et al. [24] described some of the recent development in this field.

Most of the recent available modeling efforts for characterizing unsteady frictional behavior have focused on the mixed lubrication regime. A simple model that can fully determine the behavior of friction during the complete cycle of oscillatory motion, which involves boundary, mixed, and full film lubrication regimes, is still lacking. It is worthwhile to note that Zhai et al. [25] developed a mixed film friction, considering the transient term to capture the dynamic behavior by directly solving the Reynolds equation. The solutions to the governing equations are normally very time-consuming and often exhibit sensitive convergence behavior so that they cannot readily satisfy the robust needs in control applications.

The objective of this study is to develop a simple but realistic theoretical model based on the load-sharing concept for the contact of lubricated surfaces in order to capture the previously observed dynamic friction behavior. In the present study a new approach for decoupling the Reynolds equation is proposed. The previous work by Lu et al. [13] is extended in order to capture the physical behavior of friction coefficient in lubricated line contact operating under unsteady condition. It is important to note that the inertia effect is neglected; a similar assumption is made by Zhai et al. [25], where they investigated hysteresis behavior in line contact by solving complete Reynolds equation. The model reduces to the Stribeck curve under slowly increasing velocity (so-called quasisteady). The simplicity of the developed dynamic friction model makes it useful for control application of machines in real-time.

2 Theoretical Development

2.1 Model. Operating under dynamic condition, the instantaneous friction coefficient arises from two separate origins: asperities interaction and fluid traction. Given that the inertia force in the applied load direction is negligible, the total applied load F_T is a combination of the asperity contact, hydrodynamic force, and squeeze force as appropriate contribution extent depends on the operating regime

$$F_T = F_H + F_C + F_{\text{sq}} \tag{1}$$

where F_H is the hydrodynamic force, F_C is the asperity contact force, and F_{sq} is the squeeze force.

A schematic representation of an unsteady EHL contact is shown in Fig. 1. It shows the contribution of asperities contact, hydrodynamic, and squeeze force as separate flexible elements capable of providing load-carrying capacity. The spring K_a represents the elastic deformation of asperities, the spring K_h represents the hydrodynamic action of the lubricant, and the spring K_{sq} represents the squeeze action of the lubricant. The spring K_D represents the equivalent bulk Hertzian deformation of mating bodies.

Figures 1(*b*) and 1(*c*) show the equivalent systems. In Fig. 1(*b*) we replace K_D with two springs K_{D1} and K_{D2}, representing the related deformation to asperity contact and hydrodynamic force. As the corresponding stiffness for the squeeze action of the fluid is very small compared to asperity contact and hydrodynamic action of the fluid, the system in Fig. 1(*b*) can be approximately replaced by the system in Fig. 1(*c*). Therefore, the problem of solving the unsteady elastohydrodynamic contact can be simply replaced by the problem of solving the dry line contact, considering the relevant deformation, the problem of solving lubricated line contact without surface roughness, considering its relevant deformation, and the problem of squeeze action of the fluid film. The squeeze force is obtained by integrating the squeeze pressure over the contact area. For the asperity contact and hydrodynamic forces, we use the Johnson's load-sharing concept developed for the steady case.

The complete Reynolds equation for the time-variable fluid film is

$$\frac{\partial}{\partial x}\left(\frac{\rho h^3}{12\mu}\frac{\partial p_f}{\partial x}\right) = \frac{\partial \rho h}{\partial t} + u\frac{\partial(\rho h)}{\partial x} \tag{2}$$

where h is the film thickness, μ is the lubricant viscosity, p_f is the fluid film pressure, and ρ is the fluid density. In the Hertzian line contact, the interacting surfaces undergo an appreciable amount of deformation within a rectangular contact area of the width $2a$. In an EHL line contact, the central film thickness is nearly uniform, and its width and that corresponding pressure are similar to the Hertzian dry contact [15]. The deformation equation is written as

$$h(x) = h_0 + \frac{x^2}{2R'} - \frac{4}{\pi E'}\int_{-\infty}^{+\infty} p_T(\mathrm{s})\ln(|x-s|^2)ds \tag{3}$$

where p_T denotes the sum of asperity and fluid pressure, E' is the equivalent modulus of elasticity, and R' represents equivalent radius.

Often attributed to Barus [26], the change in the viscosity with pressure takes on the following form:

$$\mu = \mu_0 e^{\alpha p_f} \tag{4}$$

Another appealing pressure-viscosity relation for the oil was given by Roelands [27] as

$$\mu = \mu_0\left(\frac{\mu_\infty}{\mu_0}\right)^{(1-(1+p_m/c_P)^Z)} \tag{5}$$

where μ_0 is the oil viscosity at the inlet temperature, $\mu_\infty = 6.315 \times 10^{-5}$ Pa.s, and p_m denotes the mean pressure for the Hertzian contact. The parameter Z represents the pressure-viscosity index as [28]

$$Z = \frac{\alpha}{[5.1\times 10^{-9}(\ln \mu_0 + 9.67)]} \tag{6}$$

where α is the pressure-viscosity coefficient. It has been shown that the effect of density change in the squeeze process is relatively small in comparison to the viscosity change effect [29].

2.2 Squeeze Term. Neglecting the surface deformation under light-load, the squeeze force can be derived by solving Eqs. (2) and (4). The pressure p_f will be replaced by p_{sq}. It is important to note that the fluid film thickness is nearly uniform over the contact area. Therefore, the central film thickness h_c is considered as a uniform film thickness over the contact area. Thus, we treat the unsteady Reynolds equation by considering the uniform film thickness. It is convenient to replace the squeeze pressure p_{sq} with an independent variable called reduced pressure q defined as

$$q(x) = \frac{1}{\alpha}\{1 - \exp(-\alpha p_{\mathrm{sq}}(x))\}$$

$$\frac{dq}{dx} = \exp(-\alpha p_{\mathrm{sq}})\frac{dp_{\mathrm{sq}}}{dx} \tag{7}$$

The solution to Eq. (7) describes the squeeze pressure in the fluid with the viscosity described by Eq. (4). The integrated form of the reduced pressure is

$$q(x) = \left\{\frac{12\mu_0}{h_c^3}\left[\frac{\partial h_c}{\partial t}\frac{x^2}{2} + c_1 x\right]\right\} + c_2 \tag{8}$$

After applying the boundary condition $q(a)=q(-a)=0$, evaluation of the constants yields $c_1=0$ and $c_2=(-12\mu/h^3)(\partial h/\partial t)(a^2/2)$. The total load is obtained by the integration of the squeeze pressure over the Hertzian contact area. The expression for the squeeze force is

$$F_{\mathrm{sq}} = \int_{-a}^{a}\frac{\ln(1-q(x)\alpha)}{-\alpha} l\ dx \tag{9}$$

where l is the length of the line contact. The resulting equation is

$$F_{\mathrm{sq}} = \frac{4al}{\alpha} - \frac{l}{\alpha}\sqrt{\frac{1+Ba^2}{B}}\ln\left(\left(\frac{\sqrt{B}a + \sqrt{1+Ba^2}}{\sqrt{1+Ba^2} - \sqrt{B}a}\right)^2\right) \tag{10}$$

where

$$B = 6\frac{\mu_0}{h_c^3}\alpha\frac{\partial h_c}{\partial t} \tag{11}$$

Another simple derivation of squeeze force is given in the Appendix [22].

Subtracting the damping load from the total applied load, the corresponding steady load is obtained as

$$F_S = F_T - F_{\mathrm{sq}} \tag{12}$$

where

$$F_S = F_C + F_H \tag{13}$$

Applying load-sharing concept of Johnson [14], the steady load can be rewritten as

$$F_S = \frac{F_S}{\gamma_1} + \frac{F_S}{\gamma_2} \tag{14}$$

where γ_1 and γ_2 are the scaling factors for asperity and hydrodynamic terms, respectively.

2.3 Elastohydrodynamic Term. The Reynolds equation for line contact considering only the steady term in the right-hand side of Eq. (2) is

$$\frac{\partial}{\partial x}\left(\frac{\rho h^3}{12\mu}\frac{\partial p_h}{\partial x}\right) = u\frac{\partial(\rho h)}{\partial x} \tag{15}$$

where p_h is the hydrodynamic pressure. The deformation equation for the hydrodynamic term is

$$h(x) = h_0 + \frac{x^2}{2R} - \frac{4\gamma_2}{\pi E'}\int_{-\infty}^{+\infty} p_h(\mathrm{s})\ln(|x-s|)^2 ds \tag{16}$$

The steady-state equation can be defined as

$$F_S = \gamma_2 l\int_{-\infty}^{+\infty} p_h(s)ds \tag{17}$$

The abovementioned equations are the same as the equations solved by Moes [16], noting that those were for smooth surfaces. In the mixed lubrication model of Johnson et al. [14], the total pressure p_T is split into the hydrodynamic pressure p_h and the asperity contact pressure p_a.

Solution of Eqs. (15)–(17) for the central film thickness can be obtained using Moes' solution, taking γ_2 in Eq. (17) to the left-hand side and in Eq. (16) out of the integration. This philosophy

can be simply applied if one replaces F_S by F_S/γ_2 and E' by E'/γ_2. These substitutions in the central film thickness relation will yield

$$\bar{h}_c\bar{U}^{-0.5} = [(\gamma_2)^{s/2}(H_{RI}^{7/3} + (\gamma_2)^{-14/15}H_{EI}^{7/3})^{(3/7)s} + (\gamma_2)^{-s/2}(H_{RP}^{-7/2} + H_{EP}^{-7/2})^{-(2/7)s}]^{s^{-1}}(\gamma_2)^{1/2} \quad (18)$$

where

$$s = \frac{1}{5}(7 + 8e^{[-2\gamma_2^{-2/5}(H_{EI}/H_{RI})]}) \quad (19)$$

with the following dimensionless parameters:

$$H_{EI} = 2.621M^{-1/5}, \quad H_{RI} = 3M^{-1}$$

$$H_{EP} = 1.311M^{-1/8}L^{3/4}, \quad H_{RP} = 1.287L^{2/3}$$

$$\bar{h}_c = h_c/R', \quad \bar{U} = \frac{\mu_0 u}{E'R'}, \quad M = W\bar{U}^{-1/2}$$

$$W = \frac{F_S}{E'R'l}, \quad L = G\bar{U}^{1/4}, \quad G = \alpha E' \quad (20)$$

2.4 Asperity Contact Term. The model of Greenwood and Williamson [17] is used for the surface asperity contact, where the contact of two rough surfaces is replaced by the contact between the equivalent rough surface with a smooth flat plate. In this study, the equivalent surface roughness parameters such as average radius of asperities β, standard deviation of asperity heights σ_s, and density of asperities n, are used. The asperity contact pressure can be expressed as

$$p_a(x) = \frac{2}{3}n\beta\sigma_s\sqrt{\frac{\sigma_s}{\beta}}E'F_{3/2}\left(\frac{h(x)}{\sigma_s}\right) \quad (21)$$

where

$$F_{3/2}\left(\frac{h(x)}{\sigma_s}\right) = \frac{1}{\sqrt{2\pi}}\int_{h(x)/\sigma_s}^{\infty}\left(s - \frac{h(x)}{\sigma_s}\right)^{3/2}e^{-(1/2)s^2}ds \quad (22)$$

The corresponding elastic deformation for the asperity contact section is the same as Eq. (16). The only difference is that $p_h(x)$ should be replaced by $p_a(x)$, and γ_2 is replaced by γ_1 in order to consider the asperity contact pressure. The steady load equation changes to

$$F_S = \gamma_1 l\int_{-\infty}^{+\infty}p_a(x)dx \quad (23)$$

Gelinck and Schipper [18] solved the governing equations for the asperity contact pressure, corresponding elastic deformation, and applied load to relate the central asperity contact pressure to the Hertzian pressure in the line contact. The only difference is that $\gamma_2 p_a(x)$ is p_a. Because of the difference in the distance between the mean of the surface and mean of the asperity, the asperity contact relation is modified by replacing h_c/σ_s by $(h_c - d_d/\sigma_s)$, where, according to Whitehouse and Archard [30], d_d is approximately $1.15\sigma_s$. The resulting equation is [18]

$$p_c = p_H[1 + (a_1\bar{n}^{a_2}\bar{\sigma}_s^{a_3}W^{a_2-a_3})^{a_4}]^{1/a_4} \quad (24)$$

where $a_1 = 1.558$, $a_2 = 0.0337$, $a_3 = -0.442$, $a_4 = -1.70$, p_c is the contact pressure of an asperity in the center of line contact, and p_H represents the maximum Hertzian pressure

$$p_H = \sqrt{\frac{F_S E'}{2\pi l R}} \quad (25)$$

Solution of Eqs. (21)–(23) coupled with the deformation equation can be obtained using the solution of Gelinck and Schipper [18] by taking γ_1 in Eq. (23) to the left-hand side and in the deformation equation out of the integration. Again, here, F_S is substituted by F_S/γ_2 and E' by E'/γ_2. In order to make Eq. (21) unchanged, n is substituted by $n\gamma_1$ to nullify the substitution of E' by E'/γ_1. If these substitutions are directly applied in Eq. (24), the following equation yields

$$\frac{2}{3}\bar{n}\bar{\sigma}_s^{3/2}\bar{F}_S F_{3/2}\left(\frac{\bar{h}_c - \bar{d}_d}{\bar{\sigma}_s}\right) = [1 + (a_1\bar{n}^{a_2}\bar{\sigma}_s^{a_3}W^{a_2-a_3}\gamma_2^{a_2})^{a_4}]^{1/a_4}\frac{1}{\gamma_1} \quad (26)$$

with the following dimensionless parameters:

$$\bar{n} = nR'\sqrt{R'\beta}$$

$$\bar{\sigma}_s = \frac{\sigma_s}{R'}$$

$$\bar{h}_c = \frac{h_c}{R'}, \quad \bar{d}_d = \frac{d_d}{R'}$$

$$\bar{F}_S = \sqrt{\frac{2\pi l R' E'}{F_S}} \quad (27)$$

2.5 Friction Coefficient. The total friction coefficient is the sum of the asperity contact friction and fluid traction effect

$$f = \frac{F_{f,H} + F_{f,C}}{F_T} \quad (28)$$

where $F_{f,H}$ is the hydrodynamic friction force, and $F_{f,C}$ is the asperity contact friction force. The asperity contact friction is assumed to follow the Coulomb's law, which is the product of an average asperity friction coefficient f_c and the load carried by the asperities F_C [13]

$$F_{f,C} = f_C F_C \quad (29)$$

For the purpose of calculating the friction force, the shear stresses are integrated over the contact area. The fluid traction expression is derived through Bair–Winer model [31]. Assuming the separation of two rough surfaces to be constant and equal to the central film thickness h_c, the hydrodynamic friction force is represented as

$$F_{f,H} = \tau_L(1 - e^{-\mu(u/h_c)/\tau_L}) \cdot 2al \quad (30)$$

where τ_L is the limiting shear stresses varying with pressure

$$\tau_L = \tau_{L0} + \beta_0 p_m \quad (31)$$

where τ_{L0} is the limiting shear stress at ambient pressure, β_0 is the rate of limiting shear stress versus pressure, p_m is the average pressure of the Hertzian contact, and μ is expressed by Eq. (5), showing its change with pressure. It is assumed that the presence of asperities in the mixed regime does not influence the hydrodynamic performance.

3 Solution Procedure

The calculation procedure is outlined as follows:

1. Assume an initial film thickness for the first time-step and input the velocity for the current step.
2. Assume a trial solution for the current film thickness.
3. Solve Eq. (A1) to obtain the fluid squeeze force.
4. With a value for the squeeze term, calculate the steady applied load F_S.
5. Solve Eq. (18) to obtain γ_2; according to Eq. (14), its relevant force F_H is F_S/γ_2.
6. Calculate for γ_1 through $1 = 1/\gamma_1 + 1/\gamma_2$.
7. Check the validity of Eq. (26).
8. Repeat steps 2 to 7 until convergence is obtained.
9. Calculate for the friction coefficient through Eqs. (28)–(30).

Table 1 Input parameters for steady and quasisteady simulation [7]

Parameter	Value
n	2.5×10^{10} m^{-2}
β	10×10^{-6} m
σ_s	0.2×10^{-6} m
E'	1.5×10^{11} Pa
μ_0	0.0815 Pa.s
R'	1.7835 m
f_c	0.20
α	1.71×10^{-8} Pa^{-1}
β_0	0.047
τ_{L0}	2.5×10^{6} Pa

10. Step up in time, enter the next velocity, and return to step 2 until final time.

4 Results and Discussions

4.1 Quasi-steady. Under harmonic oscillation, the interacting bodies are accelerating to their highest speed and then slowing down, passing through zero velocity. The oscillation frequency plays an important role in this process. If these accelerating and decelerating processes happen very slowly, then the mechanism of unsteady sliding contact at each instant can be approximated by an equivalent steady-state condition. We shall refer to this unsteady process as "quasi-steady." To investigate the quasi-steady condition, we use slowly increasing velocity from 0.0026 m/s to 0.6425 m/s to cover the full Stribeck curve and predict the friction coefficient. To validate the model, the steady and quasisteady friction of the contact simulated by the model is compared with the experimental work of Lu et al. [13]. Their experimental and analytical results pertain to steady-state. They showed good agreement between the experiments and simulation results for friction coefficient. The input parameters for the simulation are reported in Table 1; these correspond to experimental values reported in Ref. [13]. The range of speeds tested in the experiments is between 2 rpm and 500 rpm, the applied load is F_T=667 N, and the contact length is 25.4 mm. The steady and quasisteady simulations have been done over the same range. In the steady case at each time-step the simulation has been done using a specific constant velocity as input, while for the quasisteady the input velocity is slightly increasing with time.

The squeeze force can be determined using Eq. (A1). It is interesting to note that under the abovementioned operating condition, μ_{eff} is $1.1\mu_0$.Substituting μ_0 by μ_{eff} in Eq. (10) results in the same value for the squeeze force. Figure 2 compares the steady

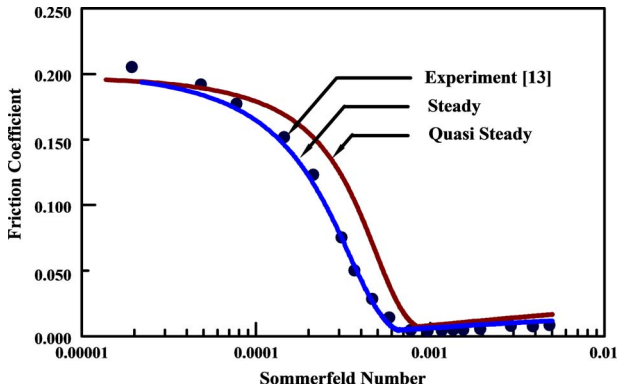

Fig. 2 Friction coefficient as a function of the Sommerfeld number (experiment versus quasisteady and steady simulations F_T=667 N and μ_0=0.0815 Pa s)

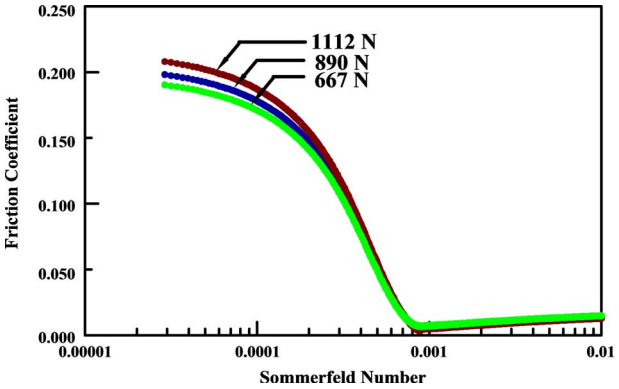

Fig. 3 Friction coefficient as a function of the Sommerfeld number (load effect μ_0=0.0815 Pa s)

experimental results with steady and quasisteady simulations. The simulation results show that the model captures the behavior of the Stribeck curve in boundary, mixed, and full lubrication regimes. The comparison of the results reveals significant insight into the squeeze phenomena in quasisteady contact of lubricated surfaces. Figure 2 illustrates that as the sliding velocity is increased in the mixed regime, the deviation from experimental steady friction behavior becomes more pronounced. Movement of interacting bodies in the normal direction is the primary cause of this deviation; the difference between the quasisteady simulation result and steady (simulation and/or experiments) is the squeeze effect. Both in the experimental results and steady simulations, the friction coefficient at each velocity is not influenced by the value at neighboring velocities. In the case of continuously increasing velocity up to 500 rpm, the friction coefficient at each step is affected by its value at previous step, causing a higher value compared with the corresponding steady case. This means that the friction coefficient is not only a function of velocity but also a function of velocity history. Physically, the fluid viscosity tends to resist against any increase in the film thickness through imposing a negative force. For this reason, for modeling, Hess and Soom [1] have considered a characteristic time lag between a changing velocity and the corresponding steady-state friction. This shift can be clearly observed in Fig. 2.

4.1.1 Effect of Load. Figure 3 shows the simulation results of friction coefficient for a range of applied load. Increasing the load causes the film thickness decrease, which increases the asperity-to-asperity interaction. As a result, the asperities tend to carry more load and friction increases. For the hydrodynamic regime, a higher load translates to a thinner film thickness. Therefore, the friction coefficient is slightly lower.

4.1.2 Effect of Viscosity. In Fig. 4 simulations correspond to three different lubricant viscosities, simulating either different inlet oil temperatures or different oil types. The lower the viscosity, the greater possibility of metal-to-metal contact, directly resulting in a higher friction coefficient. It is important to note that the thermal effects have been ignored in the model.

4.1.3 Effect of Surface Roughness. Figure 5 shows the influence of surface roughness on the friction coefficient behavior. For a rough surface with higher RMS value for asperities, the film thickness required to fill out the separation between two interacting surfaces is greater. Therefore, under the same operating condition, there must be more metal-to-metal contact for a rougher surface, which translates to a higher friction coefficient.

As we have ignored the influence of surface roughness on the performance of fluid film, there is no difference between the friction coefficients for different surface properties in the full film

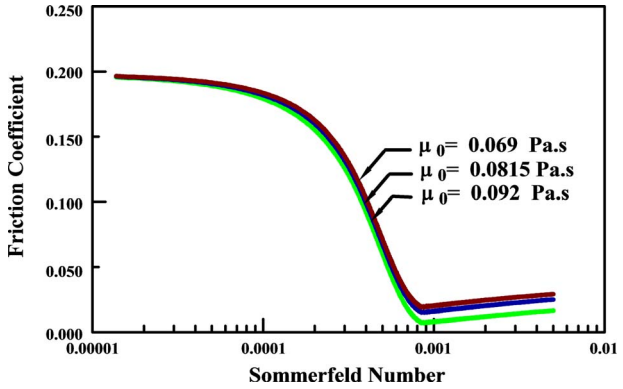

Fig. 4 Friction coefficient as a function of the Sommerfeld number (viscosity effect F_T=667 N)

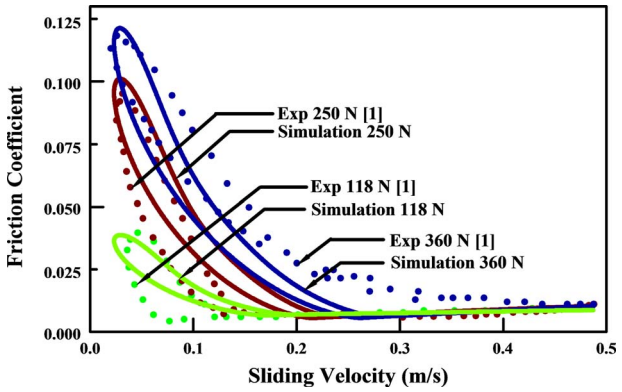

Fig. 6 Friction coefficient as a function of velocity (load effect-experiments and simulations results; f=1 Hz and μ_0 =0.322 Pa s)

lubrication regime. It is obvious that for a rough surface the transition velocity to full film lubrication is higher or it takes more time for a full film to be generated.

4.2 Unsteady Simulations. This section illustrates how the dynamic friction coefficient is predicted when oscillating frequencies in the motion are taken into account. In order to verify the model for predicting the dynamic effect we use the experimental results by Hess and Soom [1]. Their setup consists of a rotating disk in line contact with stationary flat surface both were made of 52,100 steel; the length of line contact is 19.05 mm. Light normal loads are applied to the system, causing a maximum Hertzian pressure less than 0.1 GPa. Four mineral oils with dynamic viscosities of 0.025 Pa.s, 0.102 Pa.s, 0.322 Pa.s, and 0.802 Pa.s at low temperature were used as lubricants. The velocity oscillation follows a triangular pattern under different frequencies and varies approximately linear between very small value up to around 0.5 m/s. The model developed in this study is used to predict the dynamic behavior of the friction coefficient using the same parameters reported in Ref. [1]. The pressure-viscosity relation α is assumed to be 2.2×10^{-8} Pa^{-1} for the mineral oil with the above-mentioned viscosities. The limiting shear stress at ambient pressure τ_{L0} is chosen to be 3.5×10^{6} Pa. The surface roughness parameters were obtained from Polycarpou and Soom [32]. Based on the Ref. [32], the standard deviation of surface asperities σ_s =0.45 μm, density of asperities $n=1\times10^{10}$ m^{-2}, and the average radius for the asperities β is chosen 10×10^{-6} m. It is also assumed that the Coulomb friction coefficient f_c for the asperity contact is 0.14. The simulations have been done under three different loads, i.e., 118 N, 250 N, and 360 N, with 1 Hz oscillating frequency.

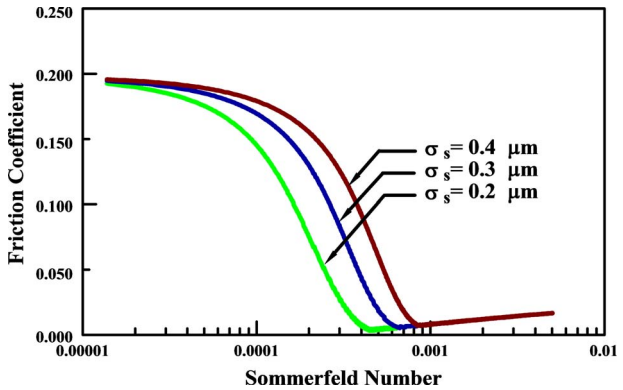

Fig. 5 Friction coefficient as a function of the Sommerfeld number (surface roughness effect F_T=500 N and μ_0=0.1 Pa s)

4.2.1 Load Effect. Figure 6 shows the simulation results and the comparison with experiments reported in Ref. [1]. The simulation results are in good agreement with the experimental results of Hess and Soom (Fig. 9 in Ref. [1]). The model predicts how slightly the friction coefficient increases after the transition from mixed to full film lubrication regime. It closely captures the experimentally observed hysteresis effect in the mixed regime, where there is high contribution of asperities that support the applied load. As the velocity increases, the film thickness increases. This implies a minus squeeze force in Eq. (A1); so the film thickness becomes less than its corresponding value of the steady-state case, resulting in a higher friction coefficient. As the velocity is decreased, the process operates in reverse and the squeeze action becomes a positive force that contributes to the load-carrying capacity. This result in a higher film thickness, which translates to a lower friction coefficient compared with the corresponding value in the steady lubrication. The physical explanation is interesting: the film thickness behaves like a damper resisting against any change in the steady-state by inducing an effect in the opposite direction. The discrepancies between the simulations and experimental results can be, in part, attributed to simplifications in the model and the uncertainty in some of the input variables used in the simulations. Another factor may be the observed is randomness in the measurement of friction coefficient [1]. It can be easily seen that for a higher load the friction coefficient will be higher. That is because of low film thickness, which causes more contribution of asperity contact in carrying out the load in the mixed film regime. For the full film regime, there is less difference in the friction coefficient between different loads. For higher load, the transition velocity from mixed to full film lubrication is higher. The results reveal that the fraction of a cycle spent in the mixed lubrication regime depends on the magnitude of the applied load.

4.2.2 Viscosity Effect. Figure 7 shows the simulation results for different values of lubricant viscosity. The trend of simulation results is in good agreement with the experimental measurements reported in Ref. [1]. The difference in the behavior of friction loop becomes slightly more pronounced especially for a higher viscosity lubricant. This can be attributed to neglecting temperature changes effect in the modeling. The "randomness of the experimental" results [1] and uncertainties in the input of the simulation parameters can be also responsible for the discrepancies. However, in general, the model captures the key physical phenomena involved. For lower viscosity, there will be more metal-to-metal contact, which accompanies more contribution of asperities in carrying out the applied load, which translates to higher friction coefficient. It can also be seen that for low viscosity, the damping effect will be lower, which is in good agreement with the proposed relation for the squeeze term. Thus, there is less friction

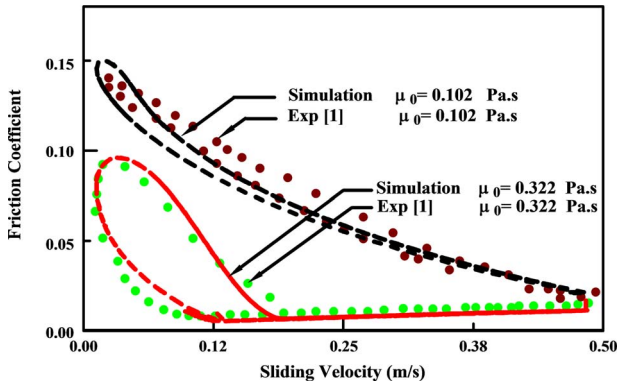

Fig. 7 Friction coefficient as a function of velocity (viscosity effect-experiments and simulations results; F_T=250 N and f =5 Hz)

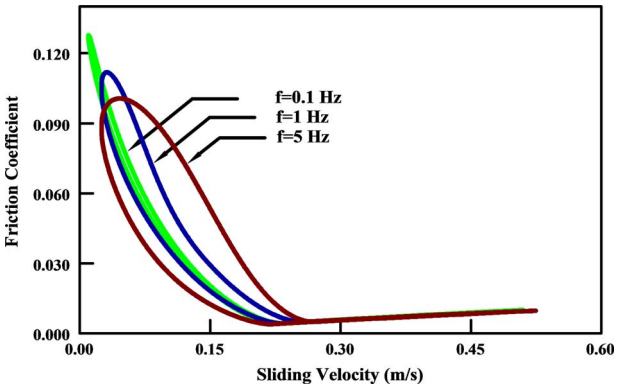

Fig. 8 Friction coefficient as a function of velocity (oscillating frequency effect F_T=200 N and μ_0=0.3 Pa s)

loop or hysteresis effect. Physically, it implies that within the context of lubrication, squeeze effect is related to the lubricant viscosity through damping.

It is obvious that the transition to full film regime will occur at higher velocities in case of using a lubricant with low viscosity. Similar to the quasisteady case, additional simulations are performed in order to investigate different parameter influences in the dynamic friction. In the following simulations, we examine the effect of imposing a sinusoidal pattern for the velocity change in a one period motion. Clearly, the extent of squeeze action is a function of fluid viscosity. The higher the viscosity of fluid, the greater is the squeeze force. The input parameters for the simulation are shown in Table 2.

4.2.3 Oscillating Frequency Effect. A series of simulations have been done to investigate the frequency and surface roughness effect. The velocity oscillates between two positive limits according to following relationship:

$$U(t) = 0.275 + 0.25 \sin(ft) \tag{32}$$

The time-variable friction is simulated by iteratively solving the governing equation as described before. Figure 8 shows simulation results for different oscillating frequencies. The hysteresis and phase-lag can be easily seen in the figure. At higher frequencies of oscillation, the size of friction loop increases, but the maximum friction is reduced. Conversely, at very low oscillating frequency, the hysteresis effect diminishes. The friction coefficient has a sharp slope and its maximum increases. The unsteady curve for a low frequency reduces to the conventional steady Stribeck curve. Physically, in case of higher oscillating frequency, the total time for one cycle oscillation is low, and there is no sufficient time for the fluid to stop flowing and this reduces the severity of friction in the boundary regime. This causes a smaller friction in the boundary regime.

It is interesting that for a specific velocity, the friction coefficient is higher at higher oscillating frequency. This means that the friction coefficient is not only a function of velocity but it also depends on the velocity history. On the other hand, it is a function of acceleration; for a positive acceleration the friction coefficient is higher than the corresponding value for the steady case while for a negative one it is smaller. This conclusion is in good agreement with the developed theory for squeeze term. For a positive acceleration the squeeze term is negative, which means that it acts like an external load. Therefore, the friction coefficient is higher. For decreasing velocity or negative acceleration the explanation is reverse. For the hydrodynamic regime, because of small rate of change in the friction coefficient, there is no significant difference between different frequencies.

4.2.4 Surface Roughness Effect. Figure 9 shows the influence of surface roughness on the elastohydrodynamic lubrication in line contact. Having the same values for the average radius β and density of asperities n for a rough surface with a higher rms value for asperities, the friction coefficient is higher in the boundary and mixed lubrication regimes. This has been shown by the model of Greenwood and Williamson [17] for the asperity contact. In the mixed lubrication area for a rough surface there is more metal-to-metal contact under the same operating conditions. The transition velocity between mixed and full film lubrications is higher for a rough surface than for a smooth one. On the other hand, for the transition to occur, the lubricant film needs to be thicker in order to prevent asperity contacts and it requires increasing the sliding velocity. It is interesting that, for a rough surface, the friction loop

Table 2 Input parameters of oscillating simulation

Parameter	Value
n	7×10^{9} m^{-2}
β	10×10^{-6} m
σ_s	0.45×10^{-6} m
E'	2×10^{11} Pa
μ_0	0.3 Pa.s
f_c	0.14
α	2.2×10^{-8} Pa^{-1}
β_0	0.047
τ_{L0}	3.5×10^{6} Pa
R'	76 mm

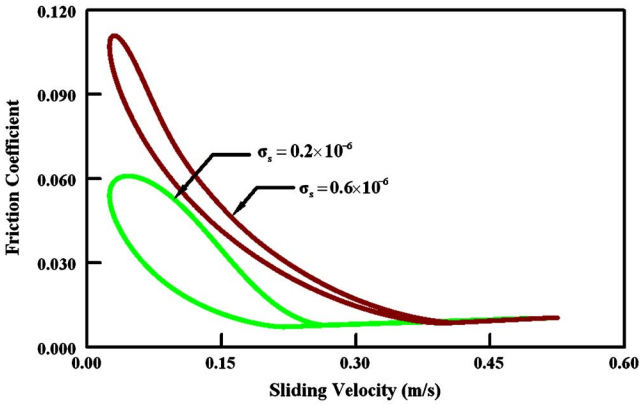

Fig. 9 Friction coefficient as a function of velocity (surface roughness effect F_T=180 N, μ_0=0.2 Pa s and f=5 Hz)

is small in comparison with a smooth one because of the greater contribution of asperities in carrying the load, and that the squeeze effect does not play any significant role. In case of full film lubrication, there is no asperity contact, which translates to very small squeeze effect, comparing to hydrodynamic film action is negligible. Therefore, after the transition from the mixed to hydrodynamic, the effect of surface disappears as the contribution of asperities in the full film regime is neglected.

5 Conclusions

A dynamic friction model is proposed for predicting the friction coefficient under both quasi-steady and unsteady operating conditions. The simulation results show that the model can realistically capture the frictional behavior in lubricated line contact operating under quasisteady and unsteady conditions. The ability of the model to accurately predict dynamic friction behavior over the different regimes reveals that the squeeze-film effect plays an important role in a dynamic friction.

Fluctuations in normal separation of two lubricated rough surfaces causes a hysteresis behavior in the friction coefficient under dynamic condition. The model captures the lag between a change in the sliding velocity and the corresponding change in friction. It should be noted that there is a sizeable loop developed in the low velocity portion of the friction curve. In this sense, the model can be considered useful for friction compensation in control applications. Higher operating frequency is accompanied by a higher rate of film thickness change, which translates to higher squeeze effect. Near the zero velocity because of the stick-slip phenomena, the friction coefficient spreads out similar to dry contact, predicting a boundary friction coefficient. This simple and robust model can be used in designing an algorithm for friction compensation in precision motion applications. An important aspect of this study is proposing the decoupling idea in order to prevent the complexity for solving the Reynolds equation in transient applications. The model is capable of further generalization to include other effects such as thermal, density, and variable loads.

Nomenclature

a = half width of Hertzian contact (m)
c_p = constant in Eq. (5), 1.962×10^8 (Pa)
d_d = distance between mean line of asperities and mean line of surface (m)
E = modulus of elasticity, (Pa)
ϑ = poisson's ratio
E' = equivalent modulus of elasticity, $=2[(1-\vartheta_1^2)/E_1+(1-\vartheta_2^2)/E_2]$ (Pa)
$F_{f,H}$ = hydrodynamic friction force (N)
$F_{f,C}$ = asperity friction force (N)
F_C = asperity contact force (N)
F_{sq} = squeeze force (N)
F_H = hydrodynamic force (N)
F_T = applied load (N)
F_S = steady force (N)
f = oscillating frequency (Hz)
f_c = friction coefficient
h = film thickness (m)
h_c = central film thickness (m)
K_D = bulk Hetzian stiffness (N/m)
K_a = asperity stiffness (N/m)
K_h = fluid hydrodynamic stiffness (N/m)
K_{sq} = fluid squeeze stiffness (N/m)
l = length of line contact, m
n = density of asperities ($1/\mathrm{m}^2$)
p_a = asperity contact pressure (Pa)
p_f = fluid total pressure (Pa)
p_h = fluid hydrodynamic pressure (Pa)
p_{sq} = fluid squeeze pressure (Pa)
p_T = sum of asperity and fluid pressure (Pa)
p_m = mean pressure of Hertzian contact (Pa)
p_H = maximum Hertzian pressure (Pa)
p_c = contact pressure of an asperity in the center of line contact (Pa)
q = reduced pressure (Pa)
R' = equivalent radius, $=1/(1/R_1+1/R_2)$ (m)
S = sommerfeld number, $=\mu V/F_T$
u = sliding velocity (m/s)
u_{ave} = average sliding velocity in half of a cycle (m/s)
Z = pressure-viscosity index
α = pressure-viscosity coefficient (1/Pa)
β = average radius of asperities (m)
β_0 = slope of limiting shear stress-pressure relation
γ_1 = hydrodynamic scaling factor
γ_2 = asperity contact scaling factor
μ = dynamic viscosity (Pa.s)
μ_{eff} = effective dynamic viscosity (Pa.s)
μ_0 = dynamic viscosity at zero pressure and room temperature (Pa.s)
μ_∞ = constant in Eq. (5), 6.315×10^{-5} Pa.s
σ_s = standard deviation of asperities (m)
τ_L = limiting shear stress (Pa)
τ_{L0} = limiting shear stress at ambient pressure (Pa)

Subscripts

1 = body 1
2 = body 2

Appendix: Effective Viscosity in Squeeze Film

Let μ_{eff} represent an effective viscosity, then, the squeeze term can be easily derived considering only the transient term in the right-hand side of Eq. (2) [16]. The result is

$$F_{\mathrm{sq}} = -\mu_{\mathrm{eff}} l \left(\frac{2a}{h_c}\right)^3 \frac{\partial h_c}{\partial t} \tag{A1}$$

Effective viscosity is calculated from Eq. (4) based on the mean pressure of the contact ($F_T/2al$). Under the light-load operating condition, the resulting value for μ_{eff} is close to μ_0. It is important to note that as α approaches zero, the effective viscosity μ_{eff} will tend to μ_0. Substituting μ_{eff} by μ_0 in Eq. (10) results in the same value obtained using Eq. (A1). The minus sign in Eq. (A1) clearly shows the damping effect of the fluid film due to changes in its thickness. If the film thickness increases, for example, due to increase in the velocity, the squeeze force will be negative. Therefore, the separation gap increases and there is no contribution to the load-carrying capacity. The damping effect in the squeeze term tends to resist a change in the steady condition result through imposing an opposite effect. The dimensionless squeeze force per unit length $\bar{F}_{\mathrm{sq}}(x)$ is obtained as

$$\bar{F}_{\mathrm{sq}} = -\bar{\mu}_{\mathrm{eff}} \left(\frac{2\bar{a}}{\bar{h}_c}\right)^3 \dot{\bar{h}}_c \tag{A2}$$

The dimensionless parameters are defined as

$$\bar{F}_{\mathrm{sq}} = \frac{F_{\mathrm{sq}}}{E'R'l}, \quad \bar{a} = \frac{a}{R'}, \quad \bar{h}_c = \frac{h_c}{R'}, \quad \bar{\mu}_{\mathrm{eff}} = \frac{\mu_{\mathrm{eff}} u}{E'R'}, \quad \bar{t} = \frac{ut}{R'} \tag{A3}$$

References

[1] Hess, D. P., and Soom, A., 1990, "Friction at a Lubricated Line Contact Operating at Oscillating Sliding Velocities," ASME J. Tribol., **112**(1), pp. 147–152.
[2] Rabinowicz, E., 1951, "The Nature of the Static and Kinetic Coefficients of Friction," J. Appl. Phys., **22**(11), pp. 1373–1379.
[3] Harnoy, A., Friedland, B., Semenock, R., Rachoor, H., and Aly, A., 1994,

"Apparatus for Empirical Determination of Dynamic Friction," Proceedings of the American Control Conference, Baltimore, MD, pp. 546–550.
[4] Lu, X. B., and Khonsari, M. M., 2007, "An Experimental Study of Grease-Lubricated Journal Bearings Undergoing Oscillatory Motion," ASME J. Tribol., **129**(3), pp. 640–646.
[5] Lu, X. B., and Khonsari, M. M., 2008, "An Experimental Study of Oil-Lubricated Journal Bearings Undergoing Oscillatory Motion," ASME J. Tribol., **130**(2), p. 021702.
[6] Greenwood, J. A., and Johnson, K. L., 1992, "The Behavior of Transverse Roughness in Sliding EHL Contacts," Wear, **153**, pp. 107–117.
[7] Greenwood, J. A., and Morales-Espejel, G. E., 1994, "The Behavior of Transverse Roughness in EHL Contacts," Proc. Inst. Mech. Eng., Part C: J. Mech. Eng. Sci., **208**, pp. 121–132.
[8] Greenwood, J. A., and Morales-Espejel, G. E., 1997, "Amplitude of the Complementary Function for Wavy EHL Contacts," Tribol. Ser., **32**, pp. 307–312.
[9] Lubrecht, A. A., Graille, A., Venner, C. H., and Greenwood, J. A., 1998, "Waviness Amplitude Reduction in EHL Line Contacts Under Rolling-Sliding," ASME J. Tribol., **120**, pp. 705–709.
[10] Venner, C. H., and Lubrecht, A. A., 1999, "Amplitude Reduction of Non-Isotropic Harmonic Patterns in Circular EHL Contacts Under Pure Rolling," Tribol. Ser., **36**, pp. 151–162.
[11] Hooke, C. J., and Venner, C. H., 2000, "Surface Roughness Attenuation in Line and Point Contacts," Proc. Inst. Mech. Eng., Part J: J. Eng. Tribol., **214**, pp. 439–444.
[12] Stribeck, R., 1902, "Kugellager Für Beliebige Belastungen," Z. Ver. Dtsch. Ing., **46**, pp. 1341–1348, 1432–1438, and 1463–1470.
[13] Lu, X. B., Khonsari, M. M., and Gelinck, E. R. M., 2006, "The Stribeck Curve: Experimental Results and Theoretical Prediction," ASME J. Tribol., **128**(4), pp. 789–794.
[14] Johnson, K. L., Greenwood, J. A., and Poon, S. Y., 1972, "A Simple Theory of Asperity Contact in Elastohydrodynamic Lubrication," Wear, **19**, pp. 91–108.
[15] Pan, P., and Hamrock, B. J., 1989, "Simple Formulae for Performance of Parameters Used in Elastohydrodynamically Lubricated Line Contacts," ASME J. Tribol., **112**(2), pp. 246–251.
[16] Moes, H., 1992, "Optimum Similarity Analysis With Application to Elastohydrodynamic Lubrication," Wear, **159**, pp. 57–66.
[17] Greenwood, J. A., and Williamson, J. B. P., 1966, "Contact of Nominally Flat Surfaces," Proc. R. Soc. London, Ser. A, **295**, pp. 300–319.
[18] Gelinck, E. R. M., and Schipper, D. J., 1999, "Deformation of Rough Line Contacts," ASME J. Tribol., **121**, pp. 449–454.
[19] Gelinck, E. R. M., and Schipper, D. J., 2000, "Calculation of Stribeck Curves for Line Contacts," Tribol. Int., **33**, pp. 175–181.
[20] Akbarzadeh, S. and Khonsari, M. M., 2008, "Performance of Spur Gears Considering Surface Roughness and Shear Thinning Lubricant," ASME J. Tribol., **130**(2), p. 021503.
[21] Harnoy, A., and Friedland, B., 1994, "Dynamic Friction Model of Lubricated Surfaces for Precise Motion Control," Tribol. Trans., **37**(3), pp. 608–614.
[22] Rachoor, H., and Harnoy, A., 1996, "Modeling of Dynamic Friction in Lubricated Line Contacts for Precise Motion Control," Tribol. Trans., **39**(2), pp. 476–482.
[23] Canudas de Wit, C., Olsson, H., Aström, K., and Lischinsky, P., 1995, "A New Model for Control of Systems With Friction," IEEE Trans. Autom. Control, **40**, pp. 419–425.
[24] Olsson, H., Aström, K. J., Canudas de Wit, C., Gäfvert, M., and Lischinsky, P., 1998, "Friction Models and Friction Compensation," Eur. J. Control, **4**(3), pp. 176–195.
[25] Zhai, X. J., Needham, G., and Chang, L., 1997, "On the Mechanism of Multi-Valued Friction in Unsteady Sliding Line Contacts Operating in the Regime of Mixed-Film Lubrication," ASME J. Tribol., **119**, pp. 149–155.
[26] Barus, C., 1893, "Isotherms, Isopeistics and Isometrics Relative to Viscosity," Am. J. Sci., **45**, pp. 87–96.
[27] Roelands, C. J. A., 1966, "Correlational Aspects for the Viscosity–Temperature-Pressure Relationship of Lubricating Oils," Ph.D. thesis, Delft University of Technology, Delft, The Netherlands.
[28] Khonsari, M. M., and Booser, E. R., 2008, *Applied Tribology Bearing Design and Lubrication*, Wiley, West Surcek, UK.
[29] Barnocky, G., and Davis, R. H., 1989, "The Influence of Pressure-Dependent Density and Viscosity on the Elastohydrodynamic Collision and Rebound of Two Spheres," J. Fluid Mech., **209**, pp. 501–519.
[30] Whitehouse, D. J., and Archard, J. F., 1970, "The Properties of Random Surfaces of Significance in Their Contact," Proc. R. Soc. London, Ser. A, **316**, pp. 97–121.
[31] Bair, S., and Winer, W. O., 1979, "A Rheological Model for EHL Contacts Based on Primary Laboratory Data," ASME J. Lubr. Technol., **101**, pp. 258–265.
[32] Polycarpou, A. A., and Soom, A., 1995, "Two Dimensional Models of Boundary and Mixed Friction at a Line Contact," ASME J. Tribol., **117**, pp. 178–184.